Research Article Vol. 62, No. 7 / 1 March 2023 / Applied Optics B63

applied optics

Designing broadband dispersive mirrors in the mid-infrared spectral range: a theoretical study

TATIANA AMOCHKINA[1,*] AND MICHAEL TRUBETSKOV[1,2]

[1]Optilayer GmbH, Watzmannring 71, 85748 Garching, Germany
[2]Max-Planck Institute of Quantum Optics, Hans-Kopfermann Str. 1, 85748 Garching, Germany
*Corresponding author: amochkina@optilayer.com

Received 30 September 2022; accepted 17 November 2022; posted 21 November 2022; published 4 January 2023

The study reports practically important and interesting results on designing dispersive mirrors (DMs) operating in the mid-infrared spectral range from 3 to 18 μm. The admissible domains of the most important design specifications, the mirror bandwidth and group delay variation, were constructed. Estimations of the required total coating thickness, thickness of the thickest layer, and expected number of layers are obtained. The results are confirmed by an analysis of several hundreds of DM design solutions.

https://doi.org/10.1364/AO.477072

1. INTRODUCTION

Modern laser applications are dependent on broadband dispersive mirrors (DMs) exhibiting a high reflectance and a desired phase shape, which control the phase of ultrafast pulses. In the mid-infrared (MIR) laser systems, short pulses propagate through various windows/crystals [for example, ZnSe, Ge, ZGP ($ZnGeP_2$), LGS (LiGaS2), and GaSe] and accumulate highly dispersive group delay GD(λ). This leads to deformation and broadening of pulse shapes (Fig. 1). The DMs enable one to compensate accumulated GD(λ), compressing temporally the broadened pulses and restoring their shapes.

Generally, the DMs for ultrafast laser applications operating in the MIR spectral ranges from 3 to 18 μm exhibit optical and non-optical properties essentially different from the DMs operating in the visible near-infrared (NIR) spectral ranges, namely, they should (1) compose layers from MIR thin-film materials (for example, Ge, ZnS, YbF_3, YF_3, and Si); (2) contain much thicker layers; (3) deal with adhesion problems due to high stresses; (4) deal with regions of the O-H absorption in the MIR range; (5) often exhibit GD(λ), increasing with the wavelength; and (6) be broadband (>0.6 octaves) to support ultrafast pulses.

(i) An overview of widely used MIR materials can be found, for example, in Ref. [1]. In the literature, various types of coatings based on well-established combinations of infrared materials have been reported: for example, $Ge/ZnS/YF_3$ anti-reflection coatings were developed in [2,3], and ZnS/YF_3 anti-reflection coatings were reported in [4,5]. Beam splitters, and anti-reflection and Fabry–Perot filters based on Ge/ZnS were recently reported [6,7]. Optical coatings composing ZnSe, BaF_2, CdTe, and PbTe for MIR astronomical applications were developed in [8–10]. Fabry–Perot multilayers composed of $ZnSe/BaF_2$ with SiO interlayers were reported in Ref. [11]. Studying and harnessing new materials and their combinations has started recently [12–16].

(ii) Typical thicknesses of layers in the MIR range are dependent on the central wavelength of the range and on the refractive index of the low-index material. For central wavelengths between 5 and 10 μm, the average layer thicknesses is expected to be between 0.8 and 1.7 μm, which is about 10 times larger than typical thicknesses in the visible NIR ranges.

(iii) Adhesion on MIR substrates requires development of the corresponding deposition techniques and optimizing process parameters. Due to large thicknesses, mechanical stresses can lead to deformation of optical components, or even to delamination/peeling off the coatings. The layer thicknesses can be reduced via the application of some design algorithms, but not significantly.

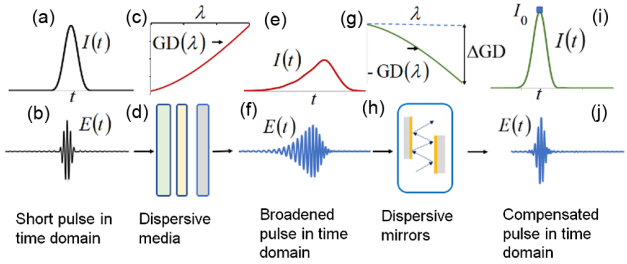

Fig. 1. Simplified pulse compensation scheme: (a), (b) short pulse propagates through a (d) set of dispersive media exhibiting (c) GD(λ) dispersion and (e), (f) broadens the pulse shapes. The pulse is (i), (j) compensated using (h) DMs providing (g) (−GD(λ)) dispersion. Designation: λ. wavelength; t, time; $I(t)$ and $E(t)$, intensity and electric field of the pulse, respectively; I_0, peak intensity.

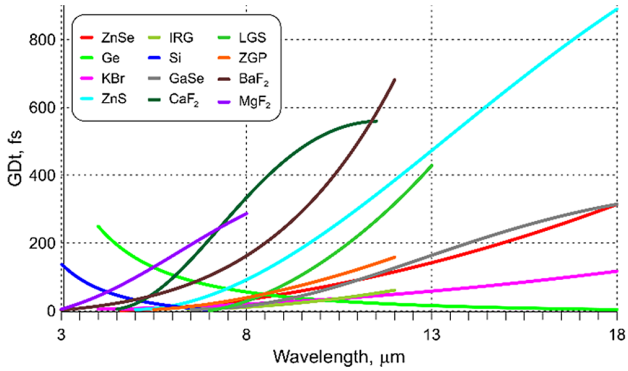

Fig. 2. GD of various typical MIR substrates/crystals used in this study calculated for 1 mm of the corresponding materials; LGS crystal was taken with a 0.1 mm thickness due to very high dispersion. The GD is plotted in spectral ranges of transparency.

(iv) The absorption of optical components in O-H absorption ranges can be reduced via optimizing of the deposition process, as well as introducing protective layers.

(v) The substrates/crystals typical for the visible NIR ranges (fused silica, glasses, Al_2O_3, BaB_2O_4, $LiNbO_3$, etc.) exhibit so-called negative GD dispersion, i.e., GD(λ) decreases if the wavelength increases. In contrast, most MIR windows/crystals exhibit GD(λ) increasing with the wavelength (Fig. 2). This affects the patterns of the structure of the designed MIR DMs.

(vi) The MIR DMs are to be broadband (>0.6 octaves), or even ultra-broadband (up to 2 octaves), to deal with MIR laser spectral ranges and provide pulse compression.

The authors are aware of only three previous publications reporting on MIR DMs: in Ref. [17], a DM provides group delay dispersion of 1500 fs^2 in the range 9–11.5 μm; in Ref. [13]; a DM with GD(λ) corresponding to 4 mm ZnSe in the range 6–11.5 μm was presented. Both DMs were implemented in a field-resolved spectroscopy laser setup [12,18]. Recently, a Si/SiO_2 MIR DM operating in the range 3–6 μm and compensating for a GD of 0.5 mm GaAs crystal was produced using the ion-beam sputtering (IBS) deposition technique [15].

The key specifications of DMs in the MIR range are the spectral bandwidth defined by its lower and upper boundaries $[\lambda_d; \lambda_u]$ (or in terms of optical octave $\Delta\lambda = \log_2(\lambda_u/\lambda_d)$and GD-variation ΔGD [Fig. 1(g)]. Typical MIR broadband ranges exceed 0.6 octaves [12,13]. The required GD-variations can take values from several femtoseconds up to 1000 fs or even 2000 fs. In a series of laser applications, the DM specifications (bandwidth and GD-variations) are formulated on the limits of the achievability. Therefore, the first question during MIR DM development is whether or not it is possible to design a MIR DM for a given combination {Δλ, ΔGD}. Until now, the corresponding admissible/forbidden combinations of the bandwidth Δλ and GD-variation ΔGD for MIR applications have not been studied. If a MIR DM for a given combination {Δλ, ΔGD} can be designed, the second question that arises is what is the expected design thickness, number of layers, and maximum thickness of layers. An empirical study on DMs operating in the visible range [19] presents achievable combinations of group delay dispersion and visible spectral range. The results from Ref. [19] are not relevant in the MIR ranges where GD dispersion rather than constant group delay dispersion is important, since the target spectral regions are very broad.

The primary goal of this study is to obtain admissible/forbidden domains of the combinations {Δλ, ΔGD}. The secondary goal is to obtain practically important estimations of expected (1) Σ—the design total physical thickness of the DM, (2) d_{max}—the thickness of the thickest layer, and (3) m—the number of layers. The admissible domain, as well as estimations (1)–(3), was obtained empirically based on the analysis of several hundreds of MIR DM design solutions. The analysis was performed for two pairs of thin-film materials, namely, Ge/YbF_3 and Ge/ZnS. Both pairs have already been used for design and production of MIR DMs [13,17].

The issues (i), (iii), and (iv) listed above concern experiments and are outside the subject of this study. The present study is theoretical and therefore concentrates on investigations of issues (ii), (v), and (vi). However, the authors have experimental experience in producing MIR coatings, including DMs [6,7,13,14,16,20], and they are convinced that the obtained results are very helpful for optical coating engineers working in the rapidly developing field of MIR DMs for laser applications.

2. METHODOLOGY

In the study, DMs for various typical MIR substrates/crystals (Fig. 2) and various spectral ranges between 3 and 18 μm were designed in the following way:

(1) DMs were designed in the ranges of transparency of the substrates to compensate the GD accumulated in 1 mm of the substrates (Fig. 2): Si [21], ZnS [22], GaSe [23], CaF_2 [24], BaF_2 [22], ZGP [25], KBr [24], IRG [26], LGS [27], MgF_2 [24], and Ge, ZnSe [20]. The only exception is the LGS crystal which, due to its very high GD-variation, was considered with a 0.1 mm thickness.

(2) For every substrate, the DM spectral range $[\lambda_d; \lambda_u]$, $\Delta\lambda > 0.6$, was chosen one by one with a 1 μm step. For example, BaF_2 is transparent in the range of 3–12 μm, then the DM ranges 3–5, 3–6, 3–10, 4–6.5, 4–7, 4–10, 5−8 μm, …, 5−11, 6–10, 6–10, 6–12 μm were considered. The ranges correspond to $\Delta\lambda = 0.74$, 1, 1.74, 0.7, 0.8, 1.32, 0.68, 1.74, 0.74, 0.87, 1, respectively. The corresponding central wavelengths of the ranges $\lambda_0 = 2\lambda_d\lambda_u/(\lambda_d + \lambda_u)$ are 3.75, 4, 4.6, 4.9, 5.1, 5.7, 6.1, 6.9, 7.5, 7.7, and 8 μm, respectively.

(3) For every substrate and every spectral range, the GD-variation was calculated as

$$\varphi(\omega) = \frac{\omega n(\omega) d}{c}, \quad \mathrm{GD}(\omega) = -\frac{d\varphi}{d\omega},$$

$$\Delta\mathrm{GD} = \mathrm{GD}(\lambda_d) - \mathrm{GD}(\lambda_u), \quad \lambda = \frac{2\pi c}{\omega}, \qquad (1)$$

where d is the substrate thickness, $n(\omega)$—is the substrate refractive index, $\{\lambda_j\}$ are evenly distributed wavelength points with a 10 nm step in the DM spectral range, and

c is light velocity. In the above BaF_2 example, the GD-variations are 31, 60, 350, 67, 89, 337, 129, 461, 290, 432, and 620 fs.

(4) For every substrate and every spectral range, DMs were designed. In the design process, gradual evolution with a deep search method of OptiLayer Thin Film Software was used [28,29]. The calculated GD with the opposite sign was taken as the target a $\hat{\mathrm{GD}}$. The target reflectance was taken to be equal to 100%. As the deviation of the current GD from the target $\hat{\mathrm{GD}}$ by an arbitrary constant C simply corresponds to the time-axis shift and does not affect the pulse shape, it is possible to relax target requirements by introducing a so-called floating constant approach [30]. The design algorithm is based on the minimization of the merit function, estimating the closeness between current and target characteristics:

$$\mathrm{MF}(X)^2 = \sum_{j=1}^{L}\left[\frac{R(X;\lambda_j) - 100\%}{0.001}\right]^2 + \sum_{j=1}^{L}\left[\mathrm{GD}(X;\lambda_j) - \hat{\mathrm{GD}}(\lambda) + C\right]^2 \to \min, \tag{2}$$

where $X = \{d_1, \ldots, d_m\}$ is the vector of layer thicknesses, and the floating constant C is automatically adjusted in the course of the optimization.

(5) For the study, two thin-film material pairs were chosen: a newly developed [13] and prospective Ge/YbF_3 combination providing a high refractive index ratio of about 2.73 and a well-established Ge/ZnS combination with a moderate refractive index ratio of 1.83. The dispersion of the refractive indices was neglected. The refractive indices of Ge, YbF_3, and ZnS were taken to be equal to 4.1, 1.5, and 2.24, respectively.

(6) A synthesis process was launched with different starting designs, including single layers, chirped mirrors, and random designs. The design reflectance can deviate from a 100% level, and the design GD exhibits inevitable oscillations around the target GD [Fig. 4(a)]. A gradual evolution algorithm with deep search [28] increases the total physical thickness and the number of layers to achieve better approximation of the target values by the DMs. From a practical point of view (issues (iii) and (iv) in the Introduction), a DM design with a minimum number of layers m, minimum total thickness Σ, and minimum thickness $d_{\max}$ should be chosen.

After the design process, a simulation of the interaction of the pulses with DMs was performed in the following way. The electric fields of the simulated pulse E and intensity I in time and spectral domains were calculated [31]:

$$E_{\mathrm{in}}(t) = \exp\left[-2\ln(2)\frac{t^2}{\tau_0^2}\right]\cdot\exp[i\omega_0 t], \quad I_{\mathrm{in}}(t) = |E_{\mathrm{in}}(t)|^2, \tag{3}$$

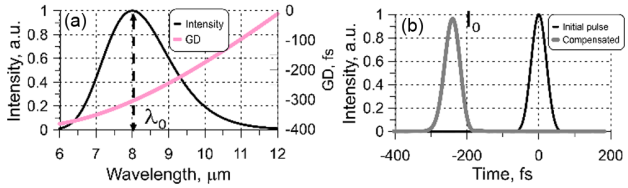

Fig. 3. Illustrating example. (a) Initial pulse and GD in a spectral domain; (b) initial and compensated pulses in the time domain. (a) GD is to be compensated with a DM.

$$E_{\mathrm{in}}(\omega) = \frac{E_0\tau_0}{2\sqrt{\ln 2}}\exp\left[-\frac{\tau_0}{8\ln 2}(\omega-\omega_0)^2\right], \quad I_{\mathrm{in}}(\omega) = |E(\omega)|^2$$
$$\omega = \frac{2\pi c}{\lambda}, \quad \omega_0 = \frac{2\pi c}{\lambda_0}, \quad E_0 = 1, \tag{4}$$

where τ_0 is the pulse duration; the intensity of the input pulse was normalized at 100%.

We denote the amplitude transmittance coefficient, phase, and transmittance of the substrate as $t_s(\omega)$, $\varphi_s(\omega)$, and T_s, respectively. Additionally, we denote the amplitude reflectance, phase, and reflectance of the DMs as $r(\omega)$, $\varphi(\omega)$, and R. After propagation through the substrate and interaction with a compensating DM, the electric field of the pulse in the time domain can be calculated:

$$E_{\mathrm{out}}(\omega) = E_{\mathrm{in}}(\omega)\, r(\omega)\, t_s(\omega), \quad r(\omega) = R(\omega)\,\exp[-i\varphi(\omega)]$$
$$t_s(\omega) = T_s(\omega)\,\exp[-i\varphi_s(\omega)]. \tag{5}$$

The electric field and intensity of the propagated pulse can be calculated using Fourier transform, providing a relationship between the spectral and the temporal representation of the laser pulse [29]. An example of the simulated pulses in the spectral and time domains is demonstrated in Fig. 3. The peak intensity of the output pulse is denoted as I_0. Due to deviations of the reflectance from a 100% level, as well as inevitable oscillations in the GD curves of the DMs, the peak intensity I_0 is lower than 100%. In addition, very large oscillations in the GD of the DMs can lead to so-called satellite pulses.

Figure 4(a) shows spectral performances of two DMs composed of Ge/YbF_3 and Ge/ZnS layers designed for the ZnS substrate in a 7–12 μm spectral range. It is seen that the reflectance curves deviate from a 100% level, and the GD curves exhibit oscillations around the target GD. The Ge/ZnS DM shows larger oscillations than Ge/YbF_3 DM. At the same time, the pulse intensity after propagation through 1 mm ZnS and interaction with the DMs is almost unchanged [Fig. 4(b)]. The peak intensities of the output pulses are 99.9% (Ge/YbF_3) and 98.7% (Ge/ZnS).

In the present study, a DM design was considered as a successful one if the peak intensity achieves more than 95%, and the output pulse does not exhibit satellites. The corresponding $\{\Delta\lambda, \Delta\mathrm{GD}\}$ combination is therefore considered as an *admissible* one. Examples of two successful designs are shown in Fig. 4. If the two conditions mentioned above cannot be fulfilled for a given $\{\Delta\lambda, \Delta\mathrm{GD}\}$ combination, i.e., if all DM designs do not provide high peak intensity values and/or exhibit satellites despite complicating the structures through a growing thickness

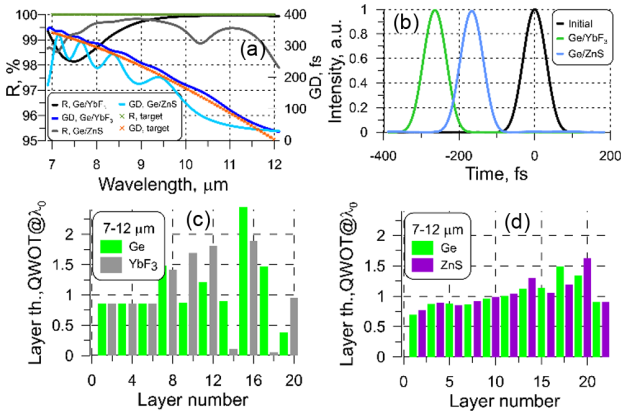

Fig. 4. Properties of two DM designs for the range of a 7–12 μm compensating GD in 1 mm ZnS: (a) reflectance and GD; (b) initial pulse and pulses propagated through DMs composed from Ge/YbF_3 and Ge/ZnS; (c) and (d) refractive index profiles of Ge/YbF_3 and Ge/ZnS DMs, respectively.

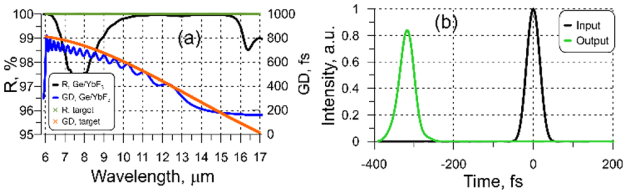

Fig. 5. Example of a DM design corresponding to a forbidden combination. Spectral range of 6–17 μm (1.5 octaves) and a GD-variation 800 fs of 1 mm ZnS: (a) reflectance and GD of a 52-layer Ge/YbF_3 solution; (b) input and output simulated pulses; the peak intensity after interaction with the substrate and DM decreases down to 81%.

and the number of layers, this combination is called *forbidden*. An example of a forbidden combination is shown in Fig. 5. A 52-layer DM design of about a 31 μm total thickness provides high reflectance values in the target spectral range of 6–17 μm and a GD oscillating near the GD target curve [Fig. 5(a)]. The intensity and peak intensity after the propagation through 1 mm ZnS and the interaction with the DM are too low [Fig. 5(b)]. The reasons for this are reflectance dips around 7–8 and 16 μm and deviation of the GD pattern from the target GD pattern. Further increasing the design thickness and complicating the design structure do not lead to better results. The considered design problem is too challenging, since the bandwidth is 1.5 octaves, and the GD-variation is about 800 fs.

7. In the course of the study, it was observed that the obtained design solutions do not depend on the starting design and have stable structural pattern. Typical DM design solutions consist of "quasi-chirped" layers and "phase" layers. Very roughly, quasi-chirped layers are responsible for the high reflectance in the broadband range, and phase layers are responsible for the phase properties. Examples of DM refractive index profiles are shown in Figs. 4(c) and 4(d). In Fig. 4(c), the first 12 layers represent a quasi-chirp, and the last eight layers present a phase part. In Fig. 4(b), the first 20 layers form the quasi-chirp, and the last two layers are phase layers. The structures of the DM profiles, as well as an estimation of the expected number of layers, will be considered in more detail in Subsection 3.4.

Analyzing several hundreds of MIR DM design structures confirmed that the most essential target characteristics are the spectral bandwidth $\Delta\lambda$ and GD-variation ΔGD. This allows one to attribute every pair ($\Delta\lambda$, ΔGD), whether it is admissible or forbidden and to plot these attributes graphically. Additionally, this enables recording and plotting the corresponding total thickness Σ, number of layers m, and thickness of the thickest layer d_{max}. The plots can be analyzed, and empirical estimations can be derived.

3. NUMERICAL RESULTS

A. Achievable GD-Variation/DM Bandwidth Combinations

Admissible {$\Delta\lambda$, ΔGD} combinations were plotted on two graphs corresponding to Ge/YbF_3 (Fig. 6) and Ge/ZnS (Fig. 7). The horizontal axis represents the bandwidth $\Delta\lambda$ in octave, and the vertical axis shows the GD-variation normalized by a characteristic $\Delta GD = 100$ fs. The points of different colors on these graphs correspond to different substrates shown in the legends. It was noticed that the admissible points form a domain marked by a gray color. Qualitatively, the admissible domain in Fig. 6 can be divided into three subdomains. The first domain, which is a rectangle with $\Delta\lambda$ from 0.6 to ≈1.25 and $\Delta GD/100$ up to ≈9, represents admissible combinations that can be achieved with a reasonable physical thickness Σ (up to 20–25 μm) and number of layers (up to 40) that is not too large.

The second subdomain, the rectangle with $\Delta\lambda$ between 0.6 and 1.25 and $\Delta GD/100 > 9$ (separated from the first domain by a dashed line in Fig. 6), represents $\Delta\lambda$ and ΔGD combinations, which are admissible, but the DM designs are difficult for production due to very large thicknesses. The realization of such designs with the total physical thickness larger than 25 μm is very challenging due to a potentially limiting factor of increase of stresses in thick layers. The question of the design production is dependent on deposition technology, including deposition techniques, process parameters, and monitoring accuracy, and therefore may vary from facility to facility. The current study provides theoretical estimations only.

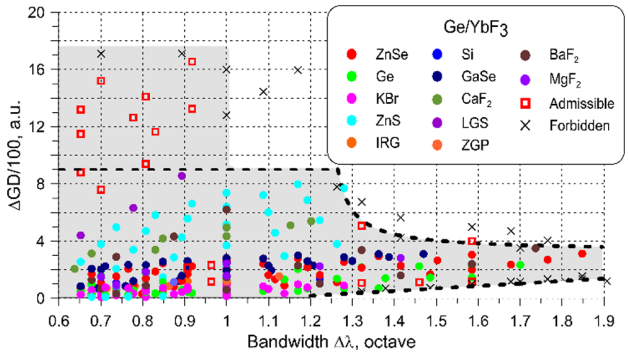

Fig. 6. Admissible domain of $\Delta GD$and the DM bandwidth $\Delta\lambda$ in the case of Ge/YbF_3 thin-film materials (gray area). The red rectangles indicate additional combinations for verification (see the text for details).

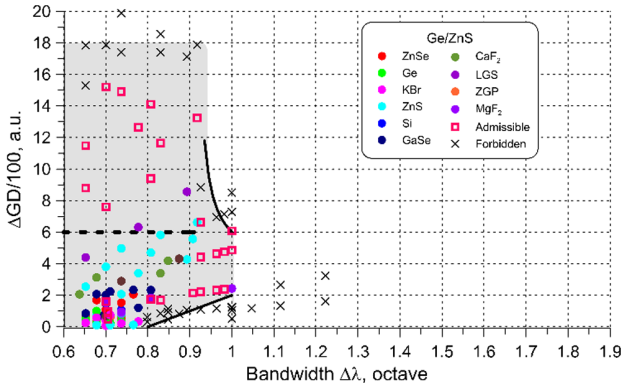

Fig. 7. Admissible domain ΔGD and the DM bandwidth Δλ in the case of Ge/ZnS thin-film materials (gray area). The red rectangles indicate additional combinations for verification (see the text of Subsection 3.1 for details).

The third subdomain is limited from the right side by Δλ of approximately 1.85–1.9 octaves that can be considered as the maximum achievable MIR DM bandwidth for the Ge/YbF_3 combination. From the top, the third domain is limited by a curve that can be empirically represented as an inverse proportionality of Δλ. In this picture, $\Delta GD/100 = \frac{0.2}{\Delta\lambda - 1.23} + 3.3$. This limiting curve predicts that it is not possible to increase both the bandwidth and GD-variation simultaneously. A product $\Delta\lambda \cdot \Delta GD$ is therefore an important parameter. An increase of the DM up to a 1.9 octave bandwidth is possible, but the GD-variations must be not large.

The third subdomain is limited from the bottom by a function that can be empirically represented as $1.72 \cdot \Delta\lambda - 1.89$. This is a very interesting result that predicts that it is not possible to increase the DM bandwidth and simultaneously specify very low GD-variations.

It should be noted here that ultra-low GD-variations ($\Delta GD < 8-10$ fs) were not considered in the present study. Designing DMs with a zero or quasi-zero GD is extremely difficult and requires additional consideration. This empirical fact can be observed not only in the MIR range, but also in the NIR and visible ranges. This phenomenon is known to some designers of multilayers for ultrafast applications, but has not been published yet, to the best of our knowledge.

After construction and qualitative explanation of the admissible area, many verification designs were calculated. Their (Δλ, ΔGD) combinations were plotted in Fig. 6 by red squares (admissible) and black crosses (forbidden). As GD targets, GDs of different substrate thicknesses and different bandwidths were considered, for example, 0.5 mm ZnS ($\Delta GD = 214$ fs) in the 7–13 μm range ($\Delta\lambda = 0.89$). A verification with BaF_2 shows that the (Δλ, ΔGD) combination of a BaF_2, 1.5 mm thickness ($\Delta GD = 506$ fs) in 4–10 μm ($\Delta\lambda = 1.32$ octaves) is admissible. At the same time, the (Δλ, ΔGD) combinations of a BaF_2, 2 mm thickness ($\Delta GD = 674$ fs) in 4–10 μm ($\Delta\lambda = 1.32$ octaves) and BaF_2, 0.1 mm thickness ($\Delta GD = 34$ fs) in 4–10 μm ($\Delta\lambda = 1.32$ octaves) are forbidden: the corresponding points (Δλ, ΔGD) lie above and below the admissible domain. All other verifications demonstrated consistency of the obtained results.

In a full analogy with a Ge/YbF_3 combination, DMs were designed and analyzed for the Ge/ZnS combination. The admissible domain is shown in Fig. 7. A comparison of the admissible domains for Ge/YbF_3 and Ge/ZnS combinations shows that the Ge/ZnS admissible domain is much smaller; the scales in two figures were chosen intentionally to be the same. The maximum achieved DM bandwidth is 1 octave. The forbidden domain on the bottom is larger: it starts at $\Delta\lambda = 0.8$ octaves and at $\Delta\lambda = 1$ octaves achieves ΔGD of 200 fs, which is not a small GD-variation value. Obviously, Ge/ZnS exhibits less potential in designing MIR DMs, mainly because of a lower refractive index ratio. Nevertheless, this combination can be used with up to one-octave MIR DMs, which can compensate up to a 1500 fs GD-variation. The dashed line in Fig. 7 shows a boundary of reasonable (Δλ, ΔGD) combinations: the thicknesses of the corresponding DM designs do not exceed 20 μm.

B. Estimation of Total Physical Thickness

During the analysis of hundreds of obtained DM solutions, it was noticed that the total thickness Σ normalized by the central wavelength λ_0 is dependent on a parameter β, which is the product of the normalized GD-variation ΔGD/100, and the bandwidth Δλ. Total thickness values normalized by the central wavelength Σ/λ_0 via β are plotted in Figs. 8 and 9 for Ge/YbF_3 and Ge/ZnS combinations, respectively. In the first approximation, the points are close to a linear function (dashed lines in Figs. 8 and 9):

$$\beta[\text{a.u.}] = \frac{\Delta GD\ [\text{fs}]}{100\ [\text{fs}]} \cdot \Delta\lambda\ [\text{octave}],$$

$$\Sigma[\mu\text{m}] \approx (0.28 \cdot \beta[\text{a.u.}] + 1.3) \cdot \lambda_0\ [\mu\text{m}], \quad \textbf{(6)}$$

in the case of Ge/YbF_3, and

$$\Sigma[\mu\text{m}] \approx (0.2 \cdot \beta[\text{a.u.}] + 1.6) \cdot \lambda_0\ [\mu\text{m}], \quad \textbf{(7)}$$

in the case of Ge/ZnS.

The same design parameters Δλand ΔGDas in the case with the admissible domain (Subsection 3.1) were used to verify Eqs. (6) and (7). The corresponding points (red squares in Fig. 8 and 9) are close to the linear functions [Eqs. (6) and (7)].

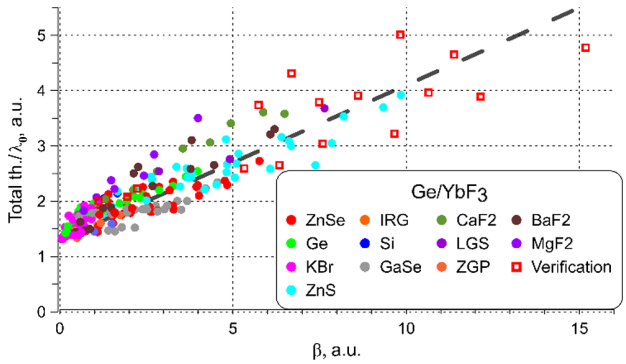

Fig. 8. Total thicknesses of DM Ge/YbF_3 designs normalized by the central wavelength versus the parameter β. The dashed line plots approximation by a linear function [Eq. (6)].

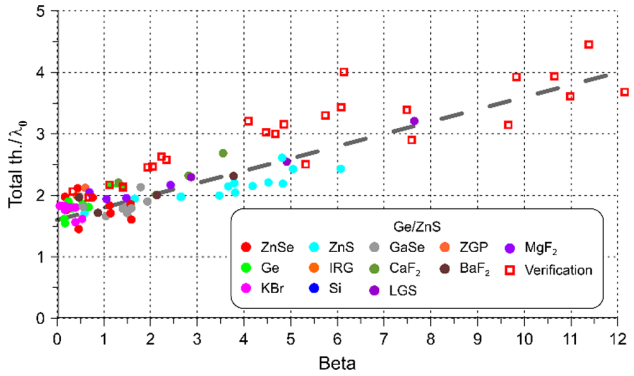

Fig. 9. Total thicknesses of DM Ge/ZnS designs versus the parameter β. The dashed line plots approximation by a linear function [Eq. (7)].

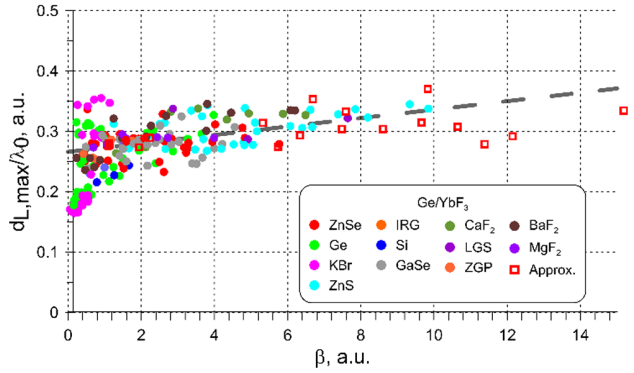

Fig. 10. Thickness of DM thickest layer $d_{\max}$ normalized by the central wavelength versus the parameter β. The dashed line plots approximation by a linear function [Eq. (8)].

C. Estimation of the Maximum Layer Thickness

The thickness of the thickest layer $d_{\max}$ is a very important parameter, since a very large layer thickness can be a limiting factor for the production process. The thicknesses of the thickest layers of the DM designs were recorded and analyzed. The thickest layer in the DM case is always a low-index layer. Its thickness $d_{\max}$ is dependent on the parameter β introduced above. The values $d_{\max}$normalized by λ_0 were plotted via the βparameter in Figs. 10 and 11, for Ge/YbF_3 and Ge/ZnS combinations, respectively. It is seen that the points can be approximated by a linear function as well. The best approximation can be provided by (dashed lines in Figs. 10 and 11):

$$d_{\max}[\mu\text{m}] \approx 0.007 \cdot (\beta[\text{a.u.}] + 38) \cdot \lambda_0\,[\mu\text{m}], \quad \textbf{(8)}$$

in the case of Ge/YbF_3 and

$$d_{\max}[\mu\text{m}] \approx 0.007 \cdot (\beta[\text{a.u.}] + 23) \cdot \lambda_0\,[\mu\text{m}], \quad \textbf{(9)}$$

in the case of Ge/ZnS.

The empirical formulas Eqs. (8) and (9) were verified additionally using the same design problems as in the case of the verification of the admissible domain. It is seen from Fig. 8 and 9 that the corresponding points (red squares) are close to the linear functions defined by Eqs. (8) and (9).

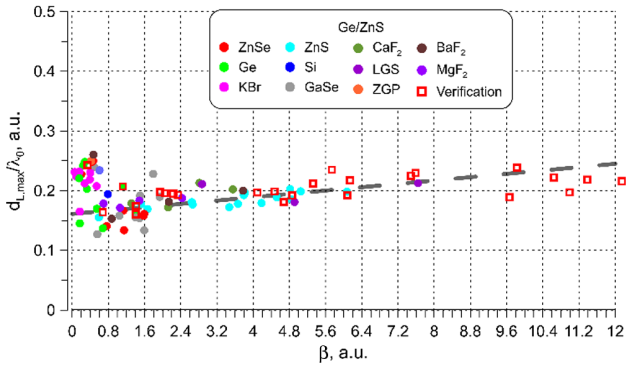

Fig. 11. Thickness of DM thickest layer $d_{\max}$ normalized by the central wavelength versus the parameter β. The dashed line plots approximation by a linear function [Eq. (9)].

D. Estimation of the Number of Layers

The number of DM design layers is dependent on the number of *quasi-chirped* and *phase* layers composing a typical DM design structure. (The discussion has been started in Section 2.) The purpose of the first quasi-chirped part is to provide a high reflectance in a broadband spectral range. A chirped structure in the current study is a quarter-wave mirror (QWM) with "smeared" quarter-wave optical thicknesses:

$$\left\{ \begin{matrix} n_H d_H \\ n_L d_L \end{matrix} \right\}_k = \frac{\lambda_0}{4} - \varepsilon + \frac{2\,(k-1)\,\varepsilon}{m-1}, \quad k = 1, \ldots m, \quad \textbf{(10)}$$

where ε is a chirp parameter n_H, n_L are the high and low refractive indices; and d_H, d_L are the thicknesses of the high- and low-index layers, respectively; k is the index of a layer; and m is the number of layers. The curly brackets designate the alternative choice of high or low refractive index layer cases. A QWM corresponds to $\varepsilon = 0$. If $\varepsilon > 0$, the high reflectance zone is broadening. At the same time, the reflectance decreases in comparison to the reflectance of the corresponding QWM having the same number of layers. An illustration with the help of 16-layer Ge/YbF_3 chirped mirrors is shown in Fig. 12(a). The high reflection zone cannot be broadened without a limit: the number of side dips, as well as their deepness, increases due to the growing number of resonances in the structure. The maximum reasonable ε values should not exceed 0.5–0.6. If the chirp parameter $\varepsilon$is fixed and the number of layers grows, the bandwidth of the high reflection zone broadens until a limit exhibiting a saturation effect. After this limit, it is not reasonable to increase the number of layers, since it will lead to an incremental increase of the reflectance on the one hand and, on the other hand, to a very large coating thickness. The process is illustrated in Fig. 12(b), where the calculations are performed for $\varepsilon = 0.3$. A reasonable number of layers providing a high reflectance in a broadband spectral range is dependent on the chirp parameter ε: this number is larger for larger ε. The reasonable number of chirp layers is 10 for $\varepsilon < 0.2$, 10–12 for $\varepsilon \approx 0.2$, 12–14 for $\varepsilon \approx 0.3$, 14–16 for $\varepsilon \approx 0.4$, and 16–20 for $\varepsilon \approx 0.5$.

An empirical estimation of the width of high reflection zone of a chirped mirror with a chirp parameter ε was obtained:

$$\Delta\lambda[\mu\text{m}] \approx \Delta\lambda_{\text{QWM}}[\mu\text{m}] + \varepsilon \cdot \lambda_0[\mu\text{m}], \quad \textbf{(11)}$$

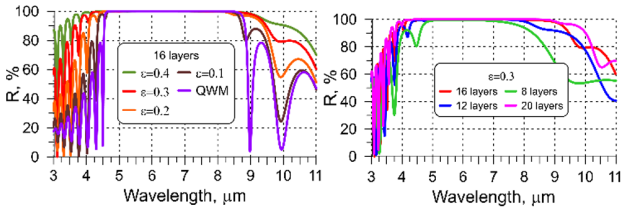

Fig. 12. (a) Reflectance curve of a 16-layer chirped mirror calculated for different chirp parameters ε; reflectance curves of chirped mirrors specified with $\varepsilon = 0.3$ and calculated for different number of layers. Thin-film combination Ge/YbF_3.

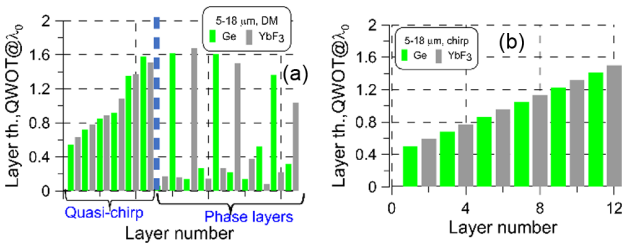

Fig. 13. (a) Refractive index profile of a 32-layer design DM solution obtained to compensate a GD of 1 mm ZnSe in the spectral range of 5–18 μm; (b) refractive index profile of a 12-layer chirped mirror designed with $\varepsilon = 0.5$.

where $\Delta\lambda_{QWM}$ is the bandwidth of the high reflectance zone of a QWM [32]:

$$\Delta\lambda_{QWM} = \lambda_0 \cdot \left(\frac{\pi}{\pi - \arccos(-\xi)} - \frac{\pi}{\pi + \arccos(-\xi)} \right)$$

$$\xi = \frac{n_H^2 + n_L^2 - 2n_H n_L}{(n_H + n_L)^2}. \quad \textbf{(12)}$$

The formula Eq. (11) can be used to estimate a required chirp parameter ε. Together with the empirical estimation above, it allows one to obtain a reasonable number of chirped layers.

The chirp parameter $\varepsilon = 0.6$ allows one to estimate the maximum achievable DM bandwidth as about 1.8 octaves. This is in good agreement with the numerical result: $\Delta\lambda = 1.85$ (5–18 μm) was achieved for $\Delta GD = 313$ fs corresponding to 1 mm ZnSe (Fig. 6). Figure 13(a) shows the DM profile of this design solution: it is seen that the first design layers form a 12-layer quasi-chirp corresponding to $\varepsilon \approx 0.5$. For comparison, a 12-layer chirp profile corresponding to $\varepsilon \approx 0.5$ is plotted in Fig. 13(b); the patterns are in good agreement.

The number of *phase* layers is strongly dependent on ΔGD, as well as on $\Delta\lambda$. Some empirical estimations based on the analysis of many hundreds of DM designs enabled us to estimate the number of phase layers, namely, 4–6 layers for ΔGD up to 200 fs and $\Delta\lambda$ between 0.6 and 1.3 octaves; seven to eight layers for ΔGD up to 400 fs and $0.6 < \Delta\lambda < 1.3$ octaves; 12–20 layers for $\Delta GD > 400$ fs and $0.6 < \Delta\lambda < 1.3$ octaves; and 10–20 layers for $\Delta\lambda > 1.3$. For the sake of convenience, the number of phase layers was plotted on the admissible diagram (Fig. 14). The number of phase layers grows either for ultra-broadband DMs or for DMs exhibiting very large GD-variations. In the example presented above, more than 14 phase layers expected, since the DM must provide the bandwidth of about 1.85 octaves. The obtained DM design includes 20 phase layers [Fig. 13(a)].

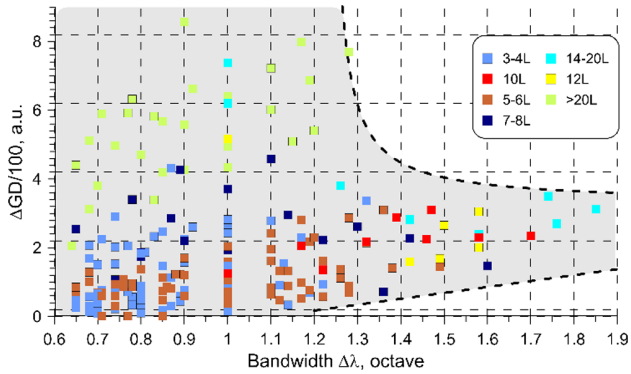

Fig. 14. Number of phase layers in Ge/YbF_3 DM structures.

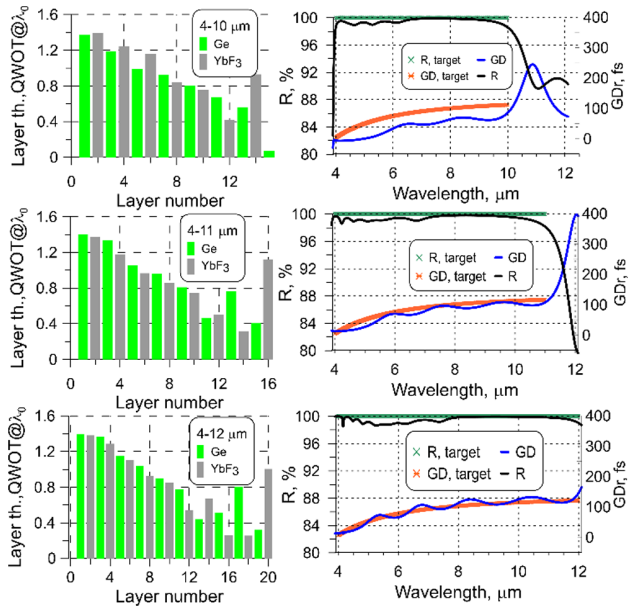

Fig. 15. Refractive index profiles (left pane) and spectral performance (right pane) of three DMs designed for compensation of a GD of 0.5 mm Ge in the spectral ranges of 4–10, 4–11, and 4–12 μm.

Figure 15 (left pane) demonstrates DM profiles for compensating 0.5 mm of Ge in the spectral ranges of 4–10, 4–11, and 4–12 μm. With broadening of the DM bandwidth ($\Delta\lambda = 1.32$, 1.45, and 1.58) and slightly increasing ΔGD(108, 112, 115 fs), the number of phase layers is 5, 5, and 8, respectively. The numbers of the first chirp layers are 10, 11, and 13, respectively. The chirp parameters are approximately 0.3, 0.4, and 0.5, respectively. The total number of layers are 15 (10 + 5), 16 (11 + 5), and 20 (13 + 7). The spectral characteristics of the design are shown in the right pane of Fig. 15: it is seen that the number of GD oscillations is larger for broader ranges, and the oscillations for broader ranges are more pronounced.

The estimation of the number of layers and analysis of the expected DM structures in the case of Ge/ZnS materials can be performed in a similar way. The maximum bandwidth [Eq. (11)] is very limited, since the main contribution is the

width of the QWM high reflection zone that is strongly dependent on the refractive index ratio [Eq. (12)]. The bandwidth of the high-reflection zone in the case of Ge/YbF_3 the combination is 0.91 octaves, while the high-reflection zone in the case of Ge/ZnS is only 0.59 octaves. With the chirp parameter ε of about 0.5, it is possible to achieve a maximum bandwidth of 1.1 octaves, which is in good agreement with the admissible domain (Fig. 7). This consideration explains why the thin-film combination Ge/ZnS cannot be used for designing broadband DMs. An analysis of multiple Ge/ZnS DM designs shows that the expected number of chirp layer is 14–16, and the expected number of phase layers is 4–8. The total number of layers lies between 18 and 24. Figure 4(d) demonstrates a typical DM refractive index profile in the case of Ge/ZnS: a DM designed for 1 mm ZnS in the range of 7–12 μm consists of 14 chirp layers and eight phase layers; the chirp parameter ε is about 0.2.

E. Some Practical Issues

In practice, DMs should be designed not just for one MIR substrate, but for a sequence of different MIR substrates and crystals involved in a laser system (Fig. 1). In this case, the total GD to be compensated can be calculated as follows:

$$\varphi_{\text{sum}}(\omega) = \frac{\omega}{c}\sum_{i=1}^{K} n_i(\omega) d_i, \qquad \text{GD}_{\text{sum}}(\omega) = -\frac{d\varphi_{\text{sum}}}{d\omega}, \quad \textbf{(13)}$$

where K is the number of substrates, and n_i and d_i are the refractive index and thickness of the ith substrate, respectively.

It is also possible that ΔGD values are very high and cannot be achieved, i.e., the given combination (Δλ; ΔGD) belongs to the forbidden zone in Figs. 6 and 7. In many cases, the problem can be solved with the help of a DM compressor, including several DMs, which allows 2, 4, 6, or 8 pulse reflections (Fig. 1). The target GD must be divided by 2, 4, 6, or 8, respectively. The GD and reflectance of the pulse compressor in the case of N bounces (N DMs) can be calculated as

$$\text{GD}_{\text{sum}}(\lambda) = N \cdot \text{GD}(\lambda), \qquad R_{\text{sum}}(\lambda) = R^N(\lambda). \quad \textbf{(14)}$$

A growing number of bounces N leads inevitably to losses of pulse energy at each bounce. A compromise between the number of bounces and feasibility issues related to a designed DM should be found by optical coating and laser engineers.

4. EXAMPLES

Some examples demonstrate the practical usage of the theoretical estimations presented above. In examples, various sets of substrates/crystals were considered; the corresponding GD(λ) and spectral ranges are plotted in Fig. 16.

Example 1. *Pulse optical path, including 1 mm LGS, 3 mm ZnSe, 5 mm Ge, 2 mm ZnS, and 1 mm GaSe operates in the range of 7–12 μm (0.78 octaves) exhibiting* ΔGD = 3430 fs.

According to Fig. 6, the combination is outside the admissible domain. Assuming four bounces ($N = 4$, $\Delta\text{GD}/100 = 8.6$, $\beta = 6.7$) and applying estimations Eqs. (6) and (7), a DM with $\Sigma = 28$ μm, $d_{\max} = 2.7$ μm, $m \approx 24-30$ can be expected. Numerically, a good solution consisting of 29 layers having a 30.6 μm thickness and 2.7 μm thickest layer was found. In the case of Ge/ZnS materials, Eqs. (7) and (9) predict solutions with $\Sigma = 26$ μm, $d_{\max} = 1.8$ μm, $m \approx 18-24$. Numerically, a 32-layer solution with a total thickness of 28.7 μm and the thickest low-index layer of 1.9 μm was obtained.

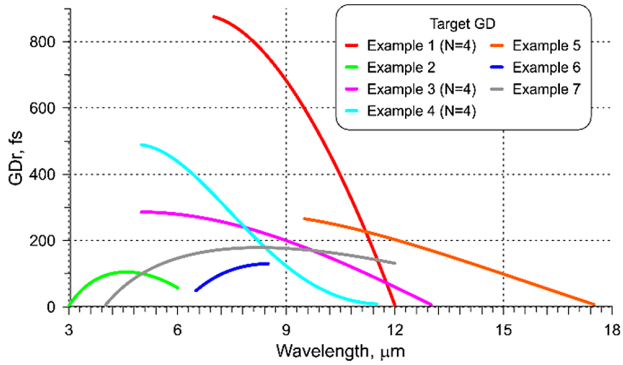

Fig. 16. Target GD used in DM design examples.

Example 2. *Pulse optical path, including 1 mm Si, 2 mm BaF2, and 1 mm ZGP operates in the range of 3–6 μm (1.0 octave) and exhibits* ΔGD = 100 fs. According to the diagram in Fig. 6, the combination is admissible. Equations (6) and (8) predict that the target specifications can be achieved with a DM design with $\Sigma = 7.2$ μm, $d_{\max} = 1.1$ μm, $m \approx 14-16$. A 16-layer solution having a total thickness of 6.9 and 0.9 μm thickest layer was found. According to the diagram in Fig. 7, the combination $\Delta\text{GD}/100 = 1$, $\beta = 1$ is in the forbidden domain and cannot be achieved with Ge/ZnS materials.

Example 3. *Pulse optical path, including 2 mm KBr, 2 mm ZnS, and 0.5 mm GaSe operates in the range 5–13 μm (1.38 octaves) exhibiting* ΔGD = 1117 fs. The combination is outside the admissible domain (Fig. 6). This means that it is not achievable with a single DM. Increasing the number of bounces (Fig. 6), the ΔGD value for one DM will be decreased. Assuming, for example, four bounces (N = 4, ΔGD = 280 fs), one obtains ΔGD = 280 fs, which belongs already to the admissible domain. A DM design having $\Sigma = 17.1$ μm, $d_{\max} = 2.1$ μm, $m \approx 24-28$ is expected according to the empirical estimations. A good solution consisting of 20 layers, having a 17.1 μm thickness and 2.1 μm thickest layer was found numerically. The combination $\Delta\text{GD}/100 = 2.8$, $\beta = 3.85$ is outside the admissible domain of Ge/ZnS materials (Fig. 7).

Example 4. *Pulse optical path, including 4 mm CaF_2, 1 mm KBr, and 2 mm Ge operates in the range of 5–11.5 μm (1.2 octaves) exhibiting* ΔGD = 1921 fs. According to Fig. 6, the combination is forbidden. At the same time, assuming four bounces ($N = 4$, $\Delta\text{GD}/100 = 4.8$, $\beta = 5.77$), a DM solution with $\Sigma = 19.2$ μm, $d_{\max} = 1.5$ μm, $m \approx 30-32$ is expected. Numerically, a 36-layer DM solution having a total physical thickness of 17.1 and 2.1 μm thickest layer was calculated. According to Fig. 7, the combination does not belong to the admissible domain of Ge/ZnS materials since the spectral range is too broad.

Example 5. *Pulse optical path, including 0.5 mm GaSe, 2 mm KBr, and 1 mm Ge operates in the spectral range of 9.5–17.5 μm (0.88 octaves) exhibiting* ΔGD = 258 fs. According to Figs. 6 and 7, the combination is admissible with Ge/YbF_3 and

Ge/ZnS materials. The expected Ge/YbF_3 DM design for the combination $\Delta GD/100 = 2.58$, $\beta = 2.27$ has $\Sigma = 23.8$ μm, $d_{max} = 3.4$ μm, and $m \approx 14-16$. Numerically, a good 15-layer DM design having a 20.5 μm thickness and a 3.1 μm thickest layer was found. In the case of Ge/ZnS materials, Eqs. (7) and (9) predict $\Sigma = 25.3$ μm, $d_{max} = 2.1$ μm, $m \approx 18-24$. A 24-layer DM solution with a total thickness of 27.4 μm and the thickest low-index layer of 2.3 μm was designed.

Example 6. Pulse optical path, including 1 mm ZGP, 0.5 mm ZnS, and 4 mm Ge operates in the range of 6.5–12 μm (0.88 octaves) exhibiting $\Delta GD = 124$ fs. According to Fig. 6, the combination is admissible. The expected parameters for the combination $\Delta GD/100 = 1.24$, $\beta = 1.1$ are $\Sigma = 15.3$ μm, $d_{max} = 2.3$ μm. A 16-layer DM design having a 16.2 μm thickness and 2.6 μm thickest layer was found. In the case of Ge/ZnS materials, the combination lies very close to the forbidden domain (Fig. 7), and target specifications cannot be achieved.

Example 7. Pulse optical path, including 4 mm ZnSe, 2 mm Ge, 1 mm KBr, and 0.5 mm GaSe operates in the range of 4–12 μm (1.58 octaves) exhibiting $\Delta GD = 349$ fs. Although the combination is admissible (Fig. 6), the point $\Delta GD/100 = 3.49$, $\Delta\lambda = 1.58$ lies very close to the boundary of the admissible domain. At the same time, a combination assuming two bounces ($N = 2$, $\Delta GD/100 = 17.5$, $\beta = 2.76$) is admissible; the expected parameters are $\Sigma = 12$ μm, $d_{max} = 1.7$ μm, $m \approx 26-28$. A 22-layer DM design having a 15.6 μm thickness and 1.95 μm thickest layer was found. In the case of Ge/ZnS materials, the combination lies outside the admissible domain (Fig. 7).

Multiple examples demonstrate excellent correspondence with theoretical predictions obtained in Section 3.

5. APPLICATION LIMITS

The theoretical estimations from Section 3 can be applied not only to thin-film combinations Ge/YbF_3 and Ge/ZnS. The formulas can be applied for DM design problems if other material pairs with close refractive indices are involved. Instead of a Ge/YbF_3 pair, combinations Ge/YF_3, Ge/MgO, Ge/DyF_3, Ge/LaF_3, Ge/MgF_2, or Ge/SiO can be used. Instead of Ge/ZnS, a combination Ge/ZnSe or PbTe/CdTe can be exploited. Additionally, the formulas can be applied in cases where the refractive index ratio is a little bit lower or higher than those considered in the present study. Larger admissible domains can be expected for combinations providing higher refractive index ratios such as PbTe/YbF_3, PbTe/DyF_3, PbTe/YF_3, PbTe/MgF_2, PbTe/SiO, and PbTe/Al_2O_3. The important questions concerning the practical realization of the DMs, including safety issues for toxic materials, as well as compatibility of these pairs in a multilayer stack, are out of scope of the present study.

Recently, an interesting combination of Si/SiO_2 materials was used to design and produce a DM compensating GD in 0.5 mm GaAs crystal [33] ($\Delta GD = 70$ fs)in the one-octave spectral range of 3–6 μm [15]. Although the combination Si/SiO_2 exhibits a smaller refractive index ratio than Ge/YbF_3 (2.54 instead of 2.73), Eqs. (6) and (8) can be used to estimate the total thickness, thickness of the thickest layer, and number

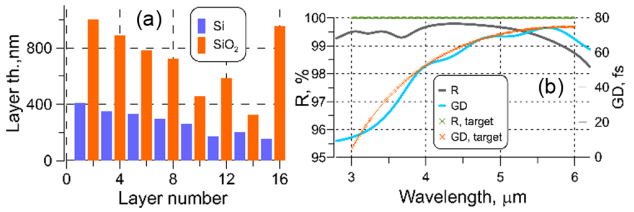

Fig. 17. (a) Refractive index profile and (b) and spectral performance of a 16-layer Si/SiO_2 DM calculated for the spectral range of 3–6 μm and compensating for a GD of 0.5 mm GaAs.

of layers. The DM design obtained in [15], consists of 21 layers and has a total thickness of 9.7 μm; the thickest layer was about 1.2 μm. Equations (6) and (8) predict the total thickness of 6.1 μm and the thickest layer of 1.1 μm. Additionally, the bandwidth of one octave corresponds to the chirp parameter $\varepsilon = 0.1$, and therefore the number of chirp layers is expected to be 10–12. The expected number of phase layers is 4–6 (Fig. 14). The total number of layers, 16–18, should be enough. Numerically, a 16-layer DM design solution was obtained in the present study (Fig. 17): the design is a typical structure consisting of 10 chirp layers and six phase layers; the pattern of the solution is similar to that in [12]. The first layers of the DM from [12] could be easily removed using advanced numerical algorithms; the total thickness could be reduced as well. The thickness of the thickest layer was 1.0 μm, which is in remarkable agreement with theoretical predictions. The total thickness of 7.9 μm is slightly larger than the predicted 6.1 μm: the difference can be attributed to slightly different ratio in the case of Ge/YbF_3 and Si/SiO_2 thin-film materials.

6. CONCLUSION

In the present study, several hundreds of MIR DM design structures were calculated and analyzed. Based on the analysis, practically important estimations of a design total thickness, the thickness of the thickest layer, and the expected number of layers were obtained. As input parameters, the estimations require the bandwidth of the DM and GD-variation to be compensated. Additionally, admissible domains of the bandwidth/GD-variation parameters were constructed for Ge/YbF_3 and Ge/ZnS thin-film combinations. The obtained formulas provide good estimations of the main DM design parameters not only for Ge/YbF_3 and Ge/ZnS pairs, but also for a large variety of thin-film combinations. The results of the study can be used by optical coating and laser engineers dealing with optical components for MIR laser applications.

Disclosures. The authors declare no conflicts of interest.

Data availability. Data underlying the results presented in this paper are not publicly available at this time but may be obtained from the authors upon reasonable request.

REFERENCES

1. M. Friz and F. Waibel, "Coating materials," in *Optical Interference Coatings* (Springer, 2003), pp. 105–130.
2. F. Lemarquis, G. Marchand, C. Amra, C. Buil, B. Cousin, and G. Otrio, "Infrared optical filters for the infrared atmospheric sounding interferometer meteorological space instrument," Appl. Opt. **38**, 4182–4188 (1999).

3. Y. Matsuoka, S. Mathonnèire, S. Peters, and W. T. Masselink, "Broadband multilayer anti-reflection coating for mid-infrared range from 7 μm to 12 μm," Appl. Opt. **57**, 1645–1649 (2018).
4. A. Ribeaud, J. Pistner, H. Hagedorn, and S. Joseph, "Infra-red multi-layer coatings using YbF_3 and ZnS in an ion beam sputtering system," in *Optical Interference Coatings Conference (OIC)* (Optica Publishing Group, 2019), paper MC.7.
5. A. V. Tikhonravov, V. G. Zhupanov, V. N. Fedoseev, and M. K. Trubetskov, "Design and production of antireflection coating for the 8–10 μm spectral region," Opt. Express **22**, 32174 (2014).
6. T. Amotchkina, M. Trubetskov, D. Hahner, P. Jacob, A. Weigel, I. Pupeza, and V. Pervak, "Fabry-Pérot based temporal standard at 8.5 μm for electro-optic delay tracking," in *The European Conference on Lasers and Electro-Optics* (2021).
7. T. Amochkina, D. Hahner, M. Trubetskov, H. Kassab, I. Pupeza, F. Krausz, and V. Pervak, "Ultra-broadband near-infrared/mid-infrared beamsplitter for bio-medical laser applications," in *Optical Interference Coatings Conference* (2022), paper TA.11.
8. G. J. Hawkins, R. Hunneman, R. Sherwood, and B. M. Barrett, "Interference filters and coatings for mid-infrared astronomy (8–30 μm)," Proc. SPIE **4842**, 43–55 (2003).
9. G. J. Hawkins, R. Hunneman, R. Sherwood, and B. M. Barrett, "Infrared filters and coatings for the high resolution dynamics Limb sounder (6–18 μm)," Appl. Opt. **39**, 5221–5230 (2000).
10. G. J. Hawkins and R. Hunneman, "Design and fabrication of infrared filters for remote sounding instrumentation," Proc. SPIE **2210**, 639–651 (1994).
11. D. Admassu, T. Durowade, R. Sellers, and S. Sivananthan, "Effect of interface grading on the optical performance of distributed Bragg reflector multilayers in Fabry-Pérot optical filters," Microsyst. Technol. **27**, 2785–2790 (2021).
12. I. Pupeza, M. Huber, M. Trubetskov, *et al.*, "Field-resolved infrared spectroscopy of biological systems," Nature **577**, 52–59 (2020).
13. T. Amotchkina, M. Trubetskov, S. A. Hussain, D. Hahner, D. Gerz, M. Huber, W. Schweinberger, I. Pupeza, F. Krausz, and V. Pervak, "Broadband dispersive Ge/YbF_3 mirrors for mid-infrared spectral range," Opt. Lett. **44**, 5210 (2019).
14. T. Amotchkina, M. Trubetskov, M. Schulz, and V. Pervak, "Comparative study of NIR-MIR beamsplitters based on ZnS/YbF_3 and Ge/YbF_3," Opt. Express **27**, 5557 (2019).
15. Y. Chen, D. Hahner, and V. Pervak, "3–6 μm dispersive mirrors compensating for dispersion introduced by the GaAs crystal," Appl. Opt. **60**, 9249–9253 (2021).
16. D. Hahner, T. Amochkina, M. Trubetskov, and V. Pervak, "Optical characterization of electron-beam evaporated Si, DyF_3, MgF_2, and MgO thin films from visible to mid-infrared ranges," in *Optical Interference Coatings* (Optica Publishing Group, 2022), paper FB–9.
17. F. Habel and V. Pervak, "Dispersive mirror for the mid-infrared spectral range of 9–11.5 μm," Appl. Opt. **56**, C71–C74 (2017).
18. A. Sommer, E. M. Bothschafter, S. A. Sato, C. Jakubeit, T. Latka, O. Razskazovskaya, H. Fattahi, M. Jobst, W. Schweinberger, V. Shirvanyan, V. S. Yakovlev, R. Kienberger, K. Yabana, N. Karpowicz, M. Schultze, and F. Krausz, "Attosecond nonlinear polarization and light–matter energy transfer in solids," Nature **534**, 86–90 (2016).
19. V. Pervak, V. Fedorov, Yu. A. Pervak, and M. Trubetskov, "Empirical study of the group delay dispersion achievable with multilayer mirrors," Opt. Express **21**, 18311–18316 (2013).
20. T. Amotchkina, M. Trubetskov, D. Hahner, and V. Pervak, "Characterization of e-beam evaporated Ge, YbF_3, ZnS, and LaF_3 thin films for laser-oriented coatings," Appl. Opt. **59**, A40–A47 (2020).
21. H. H. Li, "Refractive index of silicon and germanium and its wavelength and temperature derivatives," J. Phys. Chem. Ref. Data **9**, 561–658 (1980).
22. M. Querry, *Optical Constants of Minerals and Other Materials from the Millimeter to the Ultraviolet* (Chemical Research, Development & Engineering Center/US Army Armament Munitions Chemical Command, 1987).
23. K. Kato, F. Tanno, and N. Umemura, "Sellmeier and thermo-optic dispersion formulas for GaSe (Revisited)," Appl. Opt. **52**, 2325–2328 (2013).
24. H. H. Li, "Refractive index of alkaline earth halides and its wavelength and temperature derivatives," J. Phys. Chem. Ref. Data **9**, 161–290 (1980).
25. G. D. Boyd, E. Buehler, and F. G. Storz, "Linear and nonlinear optical properties of $ZnGeP_2$ and CdSe," Appl. Phys. Lett. **18**, 301–304 (1971).
26. SCHOTT Infrared Chalcogenide Glasses—IRG 25 Product Flyer (2017).
27. K. Kato, K. Miyata, L. Isaenko, S. Lobanov, V. Vedenyapin, and V. Petrov, "Phase-matching properties of $LiGaS_2$ in the 1025–105910 μm spectral range," Opt. Lett. **42**, 4363–4366 (2017).
28. M. Trubetskov, "Deep search methods for multilayer coating design," Appl. Opt. **59**, A75–A82 (2020).
29. M. Trubetskov and A. Tikhonravov, "OptiLayer thin film software," https://www.optilayer.com.
30. M. K. Trubetskov, V. Pervak, and A. V. Tikhonravov, "Phase optimization of dispersive mirrors based on floating constants," Opt. Express **18**, 27613–27618 (2010).
31. A. Borzsonyi, A. Kovacs, and K. Osvay, "What we can learn about ultrashort pulses by linear optical methods," Appl. Sci. **3**, 515–544 (2013).
32. S. A. Furman and A. V. Tikhonravov, *Basics of Optics of Multilayer Systems* (Frontières, 1992).
33. T. Skauli, P. S. Kuo, K. L. Vodopyanov, T. J. Pinguet, O. Levi, L. A. Eyres, J. S. Harris, M. M. Fejer, B. Gerard, L. Becouarn, and E. Lallier, "Improved dispersion relations for GaAs and applications to nonlinear optics," J. Appl. Phys. **94**, 6447–6455 (2003).